

# A Hybrid Nanotube Stamp System in Intracellular Protein Delivery for Cancer Treatment and NMR Analytical Techniques

Bowen Zhang, Bingfu Liu, Zhouji Wu, Kazuhiro Oyama, Masaomi Ikari, Hiromasa Yagi, Naoya Tochio, Takanori Kigawa, Tsutomu Mikawa,\* and Takeo Miyake\*



Cite This: *Anal. Chem.* 2024, 96, 8349–8355



Read Online

ACCESS |



Metrics & More

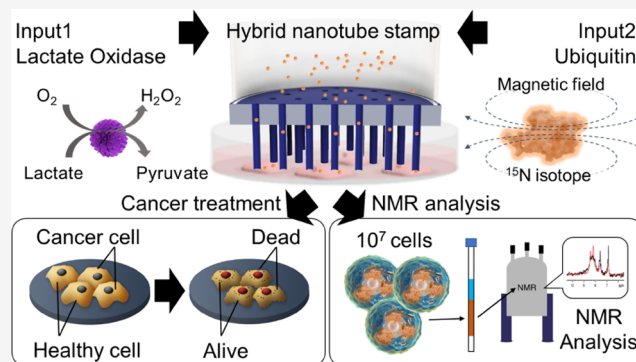


Article Recommendations



Supporting Information

**ABSTRACT:** In contrast to intracellular gene transfer, the direct delivery of expressed proteins is a significantly challenging yet essential technique for elucidating cellular functions, including protein complex structure, liquid–liquid phase separation, therapeutic applications, and reprogramming. In this study, we developed a hybrid nanotube (HyNT) stamp system that physically inserts the HyNTs into adhesive cells, enabling the injection of target molecules through HyNT ducts. This system demonstrates the capability to deliver multiple proteins, such as lactate oxidase (LOx) and ubiquitin (UQ), to approximately  $1.8 \times 10^7$  adhesive cells with a delivery efficiency of 89.9% and a viability of 97.1%. The delivery of LOx enzyme into HeLa cancer cells induced cell death, while enzyme-delivered healthy cells remained viable. Furthermore, our stamp system can deliver an isotope-labeled UQ into adhesive



cells for detection by nuclear magnetic resonance (NMR).

## INTRODUCTION

In modern biology, gene transfer is an essential experimental technique.<sup>1</sup> However, directly transfecting the target cell with a protein expression product, instead of a target gene, can avoid silencing during transcription and translation, as well as undesirable mutations caused by random DNA insertion into the target cell's genome.<sup>2</sup> Consequently, methods that can directly deliver proteins into cells are sought after, although conventional methods face challenges like uniformly delivering the necessary amount of protein for functional expression in the cell without causing toxicity.<sup>3</sup>

Chemical methods often use a cell-permeable peptide for intracellular protein delivery,<sup>4</sup> which has enabled direct reprogramming using OCT-4 proteins,<sup>5,6</sup> cancer detection and treatment with lactate oxidase,<sup>7,8</sup> and analysis of protein dynamics in living cells.<sup>9</sup> In contrast, physical methods such as electroporation,<sup>10</sup> various nanowires (like silicon,<sup>11</sup> diamond nanoneedles,<sup>12</sup> gold,<sup>13</sup> and ZnO<sup>14</sup>), and hollow needle injection (including Si,<sup>15</sup> Pt,<sup>16</sup> carbon,<sup>17</sup> and Al<sub>2</sub>O<sub>3</sub><sup>18</sup>) transport target proteins through transient holes in the cell membrane. Recently, our molecular delivery of using the metal and hybrid nanotubes (HyNTs) stamp system<sup>19,20</sup> has shown high efficiency in transporting a variety of molecules, like fluorescent molecules, oligo DNA, plasmid, and green fluorescence protein (GFP) into NIH-3T3 and HeLa cells. However, issues like safety and applicability still remain.

Here, we develop a HyNTs stamping method capable of delivering different cargoes, including calcein dye, lactate

oxidase (LOx) enzyme, and ubiquitin (UQ) protein, into multiple cells over a large area, achieving more than  $10^7$  cells for cancer treatment and NMR analysis (Figure 1). The HyNTs were created by PEDOT polymerization onto Au NTs membranes, followed by assembly with a glass tube to form a stamp for physically inserting HyNTs into cells (as shown in Figures 1 and 2a). This stamp system successfully delivers LOx enzymes to both cancer and noncancer cells, effectively eradicating cancer cells while minimizing damage to noncancer cells. Additionally, it can inject isotope-labeled ubiquitin proteins into cells for subsequent NMR signal analysis, providing insights into protein structure and dynamics. Finally, we evaluate the feasibility of our novel HyNTs nanomaterials in this stamping system.

## EXPERIMENTAL SECTION

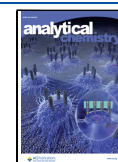
**Chemicals.** Tin chloride (SnCl<sub>2</sub>), palladium chloride (PdCl<sub>2</sub>), lithium perchlorate (LiClO<sub>4</sub>), sodium hydroxide (NaOH), hydrochloric acid (36% HCl), penicillin G potassium, streptomycin sulfate salt, and EDOT monomer were sourced from Sigma-Aldrich Chemical Co. (Massachu-

Received: November 24, 2023

Revised: April 22, 2024

Accepted: April 23, 2024

Published: May 14, 2024



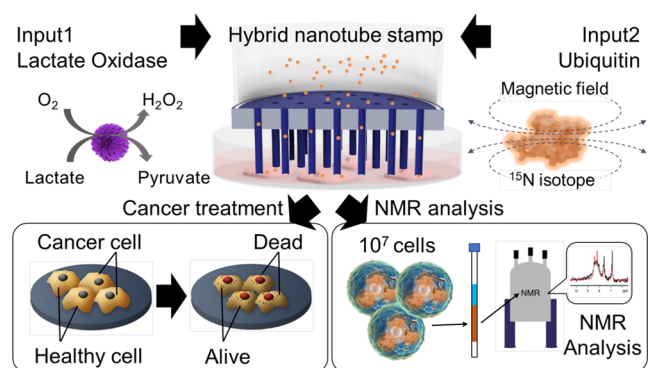


**Figure 1.** PEDOT/Au hybrid NT (HyNT) stamping for intracellular protein delivery. Delivering lactate oxidase (input 1) into cells can eliminate cancer cells, while sparing healthy cells. The delivery of isotope-labeled ubiquitin (input 2) into a large number of cells ( $>10^7$ ) facilitates NMR analysis.

sets). Dulbecco's modified Eagle's medium (DMEM), fetal bovine serum (FBS), 0.25% trypsin-EDTA, Alexa Fluor 488, and D-PBS (calcium-free, magnesium-free) were obtained from Thermo Fisher Scientific (New York State). Sodium disulfiteaurate (I) ( $\text{Na}_3[\text{Au}(\text{SO}_3)_2]$ ) and electroless gold plating solution (NC Gold II) were procured from Kojima Chemicals (Saitama, Japan). Gold surface etchant (ITO-02) was acquired from Kanto Chemicals (Tokyo, Japan). The lactate oxidase (LOx, 162.56 kDa) was prepared as previously described.<sup>21</sup> The  $^{15}\text{N}$ -labeled human ubiquitin derivative, featuring three alanine mutations (Leu8, Ile44, and Val70, designated as hUB-3A, 8.57 kDa), was provided by RIKEN Yokohama. Track-etched polycarbonate membrane (TEPM, pore size: 1000 nm, pore density:  $2 \times 10^7$  tubes  $\text{cm}^{-2}$ , thickness: 25  $\mu\text{m}$ ) was procured from it4ip company (Belgium).

**Instruments.** Scanning electron microscope (SEM) images were acquired using a JEOL SEM JSM-IT200 (JEOL, Japan). Fluorescence microscope images were obtained with a confocal microscope IX83 (Olympus, Japan). Flow cytometry data were collected using a Sysmex RF-500 (Sysmex Corporation, Japan).

**Fabrication of the PEDOT/Au Hybrid Nanotube Membrane.** Building upon our previous work,<sup>20</sup> we fabricated a PEDOT/Au hybrid nanotube (NT) membrane through a series of processes: (a) electroless gold deposition, (b) combined wet and dry etching, and (c) electrochemical PEDOT deposition. First, we deposited a gold film on the catalyst (Sn and Pd)-coated track-etched polycarbonate (TEPC) membrane using an electroless gold plating solution at 40  $^\circ\text{C}$  for 24 h. Then, the top surface of the Au nanolayer on the membrane was etched using aqua regia ITO-02 at 24  $^\circ\text{C}$  for 4.5 min. This was followed by dry etching of the exposed polycarbonate with reactive ion etching equipment (RIE-10NR, SAMCO, Japan) at 150 W for 30 min to create Au NTs. Subsequently, the Au NT membrane was immersed in a solution containing 0.05 mM EDOT and 0.1 mM  $\text{LiClO}_4$ . A voltage of 1 V was applied for 150 s using a potentiostat system with a platinum mesh counter electrode and an Ag/AgCl reference electrode to form the PEDOT on the Au NTs. The membrane was then washed twice with alcohol and twice with distilled water, followed by drying with DME compressed gas. Finally, the geometry of the PEDOT/Au NTs was verified using a scanning electron microscope.

**Cell Culture.** For our experiments, we utilized HeLa cells (RCB0007; National Research and Development Corporation RIKEN BioResource Research Center, Japan) and mesenchymal stem cells (MSC) (CellSource, Japan) as adhesive cells. The HeLa cells were cultured in Dulbecco's modified Eagle's medium supplemented with 10% fetal bovine serum, 0.0588 g  $\text{L}^{-1}$  penicillin G potassium, and 0.1 g  $\text{L}^{-1}$  streptomycin sulfate salt. The MSC cells were cultured in MSC complete growth medium. Additionally, we employed a donut-shaped dimethylpolysiloxane (PDMS) mold featuring a central hole. The diameters of this hole were matched with those of the PEDOT/Au NTs stamps (4.5, 9.0, and 18 mm). For cell suspension preparation, we utilized 0.25% trypsin and evenly dispersed the cell suspension on a PEDOT-molded Petri dish. The cells were then incubated in a 5%  $\text{CO}_2$  environment at 37  $^\circ\text{C}$ .

**NMR Measurements.**  $^{15}\text{N}$ -labeled ubiquitin was introduced into cells using our HyNTs stamp. The treated cells were detached with trypsin and collected into a 15 mL tube. Through centrifugation (300g, 3 min), the cells were washed three times with EP buffer to remove any extracellular ubiquitin. The cells were then resuspended in 150  $\mu\text{L}$  of EP buffer and immediately frozen in liquid nitrogen. After thawing at room temperature, the cells were disrupted by sonication and subsequently centrifuged (20,000g, 30 min, 4  $^\circ\text{C}$ ) to procure clear cell extracts. NMR experiments were conducted at 37  $^\circ\text{C}$  using a Bruker Avance III 600 MHz spectrometer, equipped with a cryogenic TCI probe head. Sequential 2D 1H– $^{15}\text{N}$  SOFAST–HMQC spectra were recorded.<sup>22</sup> For the ubiquitin solution measurements, the concentration was maintained at 0.1 mM.

## RESULTS AND DISCUSSION

**Improved Hybrid NTs Stamping for Large-Area Injection.** As outlined in our prior work,<sup>20</sup> the NTs stamp can be inserted into cells using a manual manipulator, with cell observation utilizing phase difference (PD) and differential interference contrast (DIC) for NTs (Figure 2a). By focusing on the top and bottom adhesive cells with PD, we assess the average cell height. The NTs were inserted from the cell top to the target position, correlating to the NTs' insertion depth, primarily set at 2  $\mu\text{m}$ , with an insertion duration of approximately 30 s. During insertion, target molecules were delivered into the cells through the NT ducts.

In these experiments, the PEDOT was electrochemically coated onto the surface of the Au NTs membrane. Subsequently, we examined the nanostructures of the hybrid NTs membrane's top (Figure 2b) and bottom (Figure 2c) surfaces using SEM. The inner and outer diameters of the hybrid NTs were 0.7 and 1.2  $\mu\text{m}$ , respectively, indicating that around 40 nm thick PEDOT nanofilm can coat the original Au NTs surface (inner diameter: 0.78  $\mu\text{m}$ , outer diameter: 1.0  $\mu\text{m}$ , pore density:  $2 \times 10^7$  tubes  $\text{cm}^{-2}$ , NT height: 5  $\mu\text{m}$ ). Coating the PEDOT on the membrane offers two advantages: it provides an adhesive interface between the hybrid PEDOT/Au membrane and glass tube surface when using UV-curing resins as glue, and it helps prevent target solution leakage from NT ducts into the culture medium. In fact, although the calcein solution flowed at  $6.55 \times 10^{-5}$  ml/(min $\cdot$ mm $^2$ ) through original Au NTs, the flow rate decreased to  $1.31 \times 10^{-5}$  ml/(min $\cdot$ mm $^2$ ) in hybrid NTs (Supporting Figure S1), suggesting a reduction of leaked solution to only 0.1 mL at 30 min with an 18 mm diameter stamp.

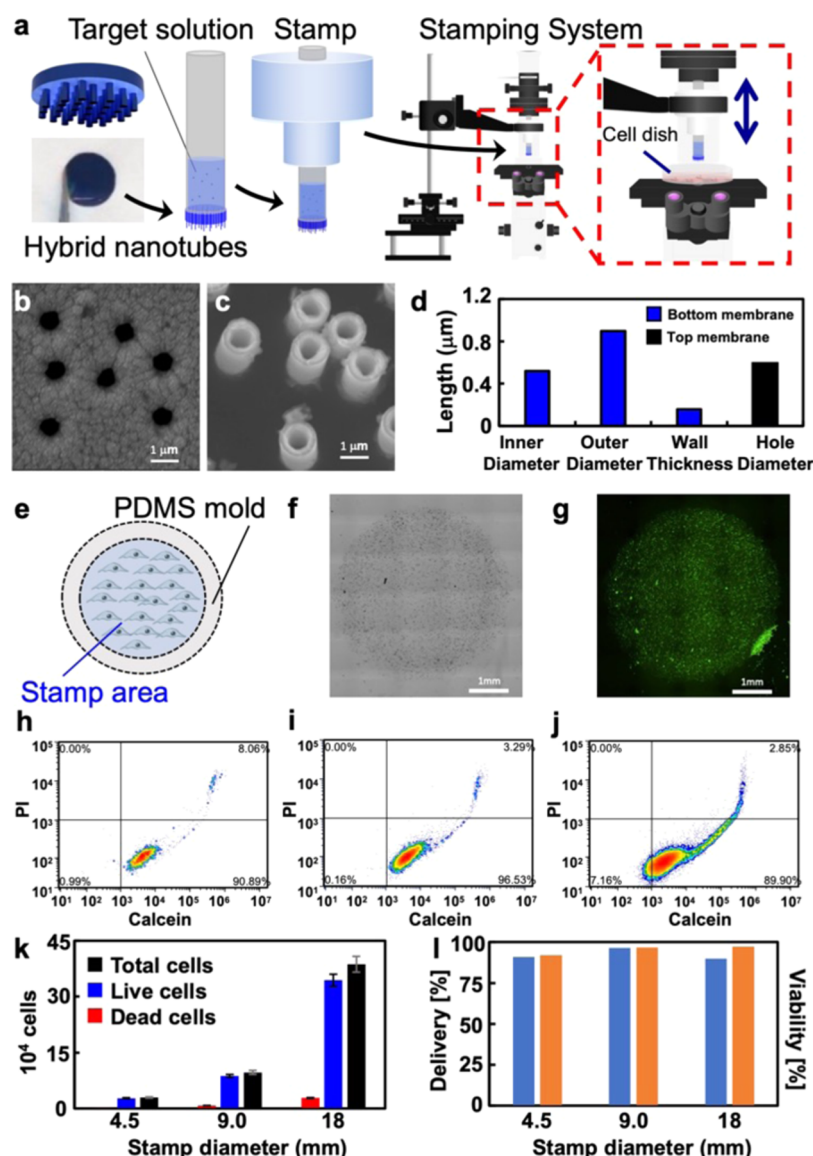


**Figure 2.** Enhanced hybrid nanotube (NT) stamping for large-area injection. (a) Illustration and photo of the PEDOT/Au NT membrane and stamping system. (b, c) Scanning electron microscopy (SEM) images of the hybrid NTs, showing the bottom (b) and top (c) views. (d) Estimations of inner diameter, outer diameter, and wall thickness of the hybrid NTs derived from SEM images. (e) Diagram of cell culture in polydimethylsiloxane (PDMS) designed to create an optimal area for stamping. (f, g) Optical (f) and fluorescence (g) images of cells delivered with calcein in a 4.5 mm area. (h–j) Flow cytometry analysis of cells treated with NT stamps of diameters 4.5 mm (h), 9 mm (i), and 18 mm (j). (k, l) Compiled flow cytometry data summarizing cell count, delivery efficiency, and cell viability. The error bar represents the standard deviation of the measured values ( $n = 5$ ).

We delivered a small cargo of calcein fluorescence dye into HeLa cells using the hybrid NT stamp of different diameters (4.5, 9.0, and 18 mm). Post-delivery, we observed optical (Figure 2f and Supporting Figure S2a–f) and fluorescence (Figure 2g and Supporting Figure S2g–i) images. After a 20 min incubation period to repair the cell membrane damaged by NTs insertion, PI dye staining was performed to identify dead cells. The counting of calcein-delivered, PI-stained, and total cells was conducted through FACS measurements (Figure 2h–l). Delivery and viability are defined as follows: Delivery (%) = (calcein-delivered cells/total cells)  $\times$  100 and Viability (%) = (1-dead cells/total cells)  $\times$  100, where dead cells are the PI-stained cells. Using a 4.5 mm NTs stamp, calcein dye was injected into  $0.227 \times 10^5$  cells with a delivery efficiency of 91% and cell viability of 92%. Increasing the stamp size resulted in more delivered cells:  $0.872 \times 10^5$  cells with a 9 mm stamp and

$3.44 \times 10^5$  cells with an 18 mm stamp. The delivery and viability rates (96.5 and 96.7% with the 9 mm stamp, 89.9 and 97.1% with the 18 mm stamp) were comparable to those with the 4.5 mm stamp. These results demonstrate that the hybrid NTs stamp can deliver molecules into over  $10^5$  cells in a single stamping with high delivery efficiency and viability.

**LOx Enzyme Delivery for Cancer Treatment.** Lactate oxidase (LOx) is an enzymatic biocatalyst that catalyzes the conversion of L-lactate and oxygen into pyruvate and hydrogen peroxide ( $H_2O_2$ ). In our previous works,<sup>21,23–25</sup> we utilized this biocatalyst for biofuel cell and sensor applications, focusing on the energy conversion from lactate chemicals to electricity. In these experiments, we delivered the functional LOx enzyme into two types of adhesive cells: healthy MSC cells and cancerous HeLa cells, to investigate cellular functions based on the concentration of the delivered LOx.

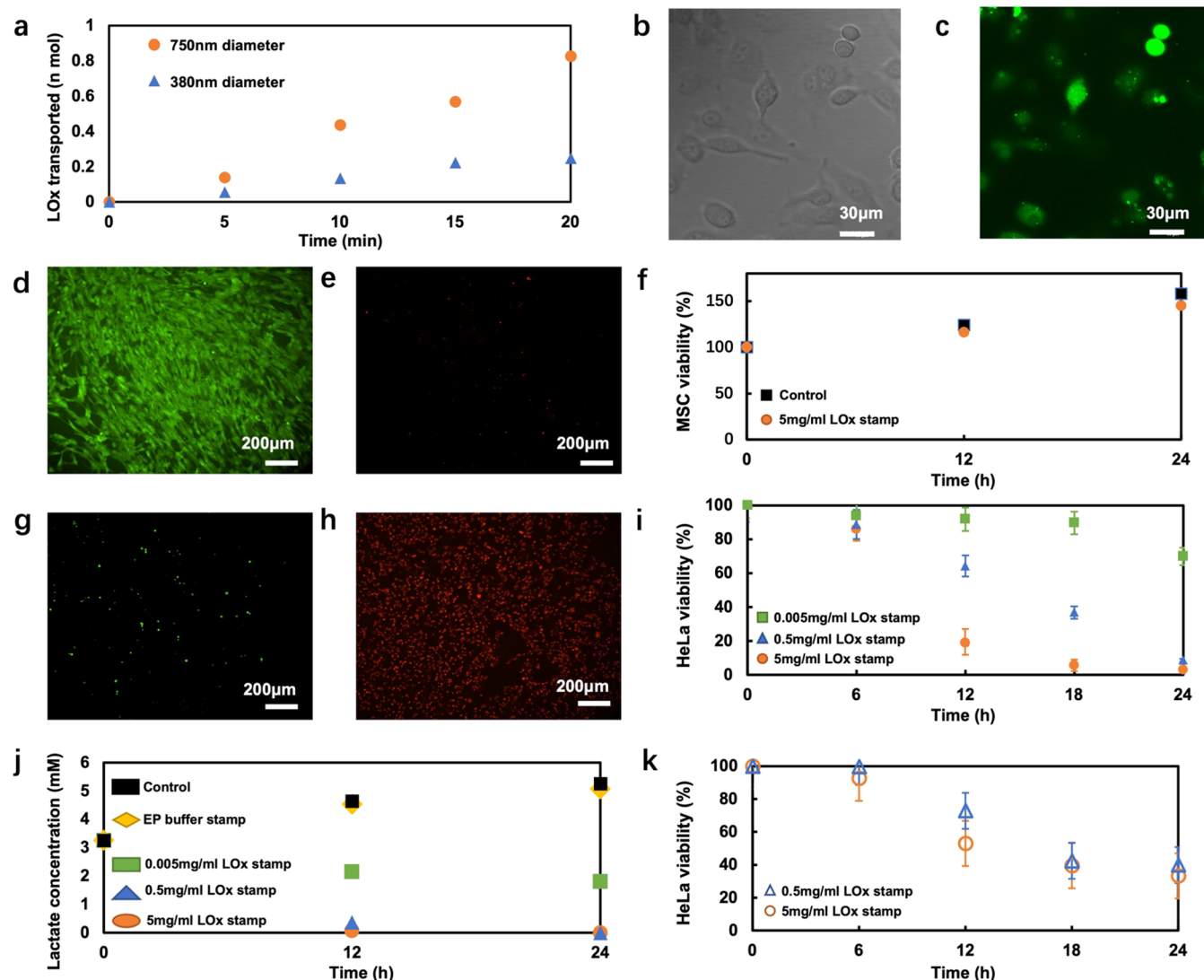


**Figure 3.** LOx enzyme delivery for cancer treatment. (a) Quantification of transported Alexa Fluor 488-stained LOx using nanotube membranes of different diameters. (b, c) Optical (b) and fluorescence (c) images showing the cells 10 min after delivery of Alexa Fluor 488-stained LOx. (d, e) Fluorescence images of MSC cells stained with Calcein-AM (d) and PI (e) 24 h after culturing the delivered cells. (f) MSC cell viability post-LOx delivery. (g, h) Fluorescence images of HeLa cells stained with Calcein-AM (g) and PI (h) 24 h after culturing the delivered cells. (i) HeLa cell viability following LOx delivery. The error bar represents the standard deviation of the measured values ( $n = 3$ ). (j) Changes in L-lactic acid concentration in the culture medium over time, following LOx delivery into HeLa cells under various conditions. (k) HeLa cell viability after exposure to LOx enzymes in the culture medium (triangle: 0.5 mg/mL and circle: 5.0 mg/mL). The error bar represents the standard deviation of the measured values ( $n = 3$ ).

To calibrate the flow of LOx enzymes through the NTs stamp, we constructed a stamp for the source chamber to measure the amount of LOx transported through the NTs membrane (diameter: 4.5 mm). When the stamp contacts the collection chamber in stirred phosphate-buffered saline (PBS) solution, LOx molecules diffuse from the highly concentrated source chamber through the NTs membrane into the collection chamber. In our experiment, the source chamber contained an Alexa Fluor 488-labeled LOx solution at a concentration of 5 mg/mL (31.25  $\mu$ M). As previously described,<sup>19</sup> its flux is defined as  $J = DC(\pi^2 n / \pi R^2) / l$ , where  $D$  is the diffusion coefficient,  $C$  is the LOx concentration,  $\pi^2$  is the inner diameter of the NTs,  $n$  is the number of NTs on the membrane area ( $2.2 \times 10^7$ ), and  $l$  is the film thickness (25  $\mu$ m). As shown in Figure 3a, the flow rates of LOx enzymes through the NTs membrane were  $J = 1.45 \times 10^{-3}$  nmol s<sup>-1</sup>

cm<sup>-2</sup> for NTs with a 380 nm inner diameter and  $J = 3.35 \times 10^{-3}$  nmol s<sup>-1</sup> cm<sup>-2</sup> for NTs with a 750 nm inner diameter. Although these values were lower than our previous measurements using calcein due to the lower concentration and larger size of the target LOx enzyme, they were sufficient for cell delivery. Indeed, we confirmed the delivery of fluorescence-labeled LOx into HeLa and MSC cells with an efficiency of 95% (Figure 3b,c and Supporting Figures S3b and c). MSC cells treated with a 5 mg/mL LOx stamp grew at the same rate as control cells for 24 h (Figure 3d–f). However, HeLa cancer cells treated with 5 mg/mL LOx died significantly, with viabilities of 85.9% at 6 h, 18.8% at 12 h, 5.5% at 18 h, and 3.0% at 24 h (Figure 3g–i). The viability of HeLa cells can be modulated by adjusting the post-delivery culturing time and LOx concentration: 93.8% at 6 h, 91.8% at 12 h, 89.7% at 18 h, and 86.9% at 24 h with 0.05 mg/mL; and 88.7% at 6 h, 64.2%

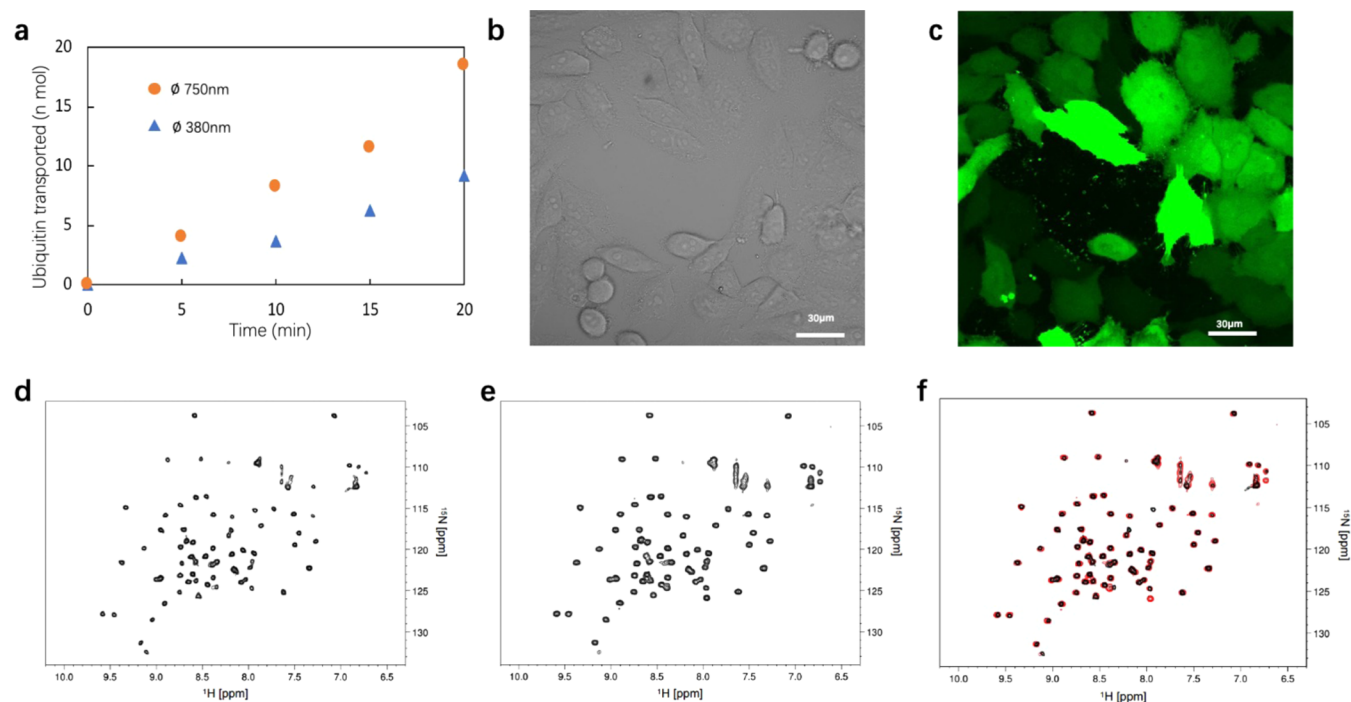


**Figure 4.** Ubiquitin protein delivery for NMR detection. (a) Quantity of transported Alexa Fluor 488-stained Ubiquitin using nanotube membranes of varying diameters. (b, c) Optical (b) and fluorescence (c) images showing cells after delivery of Alexa Fluor 488-stained Ubiquitin for 10 min. (d–f) NMR spectra of  $^{15}\text{N}$ -labeled ubiquitin: (d) from cell lysate, (e) in vitro, and (f) combined NMR spectra from (d) (black) and (e) (red).

at 12 h, 36.8% at 18 h, and 8.7% at 24 h with 0.5 mg/mL (Figure 3i and Supporting Figure S4). Since LOx reacts with lactate to produce the oxidizing agent  $\text{H}_2\text{O}_2$ , we measured lactate concentration in the medium after culturing the delivered HeLa cells under various conditions. The original medium contained 3.27 mM lactate, which increased to 5.26 mM after 24 h of cell culture (Figure 3j). In control experiments using EP buffer-stamped HeLa cells, lactate concentration also rose to 5.06 mM after 24 h. However, when we delivered LOx at concentrations of 0.05, 0.5, and 5.0 mg/mL into the cells, lactate concentration dramatically decreased. After 24 h, lactate concentrations were nearly zero with 0.5 and 5.0 mg/mL LOx stamps, while 1.81 mM lactate remained with a 0.05 mg/mL LOx stamp. Interestingly, cell viabilities at 12 h with 0.5 and 5.0 mg/mL LOx stamps differed significantly, even though lactate in the extracellular medium was nearly depleted at 12 h (Figure 3i). As a control, we injected LOx directly into the culture medium without intracellular delivery. After 24 h, viabilities of 40 and 33% were observed using 0.5 and 5.0 mg/mL LOx, respectively, much higher than those of cells with intracellularly delivered LOx (Figure 3k). These results indicate that intracellularly delivered LOx enzymes efficiently killed cancer cells.

**$^{15}\text{N}$ -Labeled Ubiquitin Protein Delivery for NMR Detection.** To analyze complex protein structures and their interactions within cells, we demonstrate the delivery of  $^{15}\text{N}$  isotope-labeled ubiquitin proteins into HeLa cells using our hybrid NTs stamp. In comparison with the LOx enzyme, the ubiquitin protein is 20 times smaller in molecular weight, allowing for a significant increase in concentration (up to 0.34 mM). Similar to the LOx flux experiments, we measured the flux  $J$  of Alexa Fluor 488-labeled ubiquitin through the stamp membranes using NTs with inner diameters of 380 and 750 nm. The flux values were  $0.133 \text{ nmol s}^{-1} \text{ cm}^{-2}$  for the 380 nm

NTs and  $0.219 \text{ nmol s}^{-1} \text{ cm}^{-2}$  for the 750 nm NTs. These values were higher than those obtained with LOx enzymes but lower than the results with green fluorescence protein (GFP, 25 kDa) at 0.8 mM.<sup>20</sup> We observed that the protein flow rate through the NTs stamp was more influenced by concentration than by molecular weight relative to the diffusion constant.

To detect NMR signals from  $^{15}\text{N}$ -labeled ubiquitin proteins, over  $10^7$  cells were required. Our stamp, featuring an 18 mm diameter NTs membrane, can inject target proteins into  $3.4 \times 10^5$  cells at a time, necessitating 50 stamping repetitions for adequate protein delivery. Post-stamping, we verified the presence of Alexa Fluor 488-labeled ubiquitin in HeLa cells through optical and fluorescence imaging (Figure 4b,c). Additionally, we extracted 100  $\mu\text{L}$  of cell suspension post-protein delivery and used flow cytometry to count total cell numbers, staining with Calcein-AM to identify live cells. The delivered and collected cells totaled  $1.8 \times 10^7$  with a viability of 88.94% (Supporting Figure S5). After washing the cells three times to remove extracellular ubiquitin and freezing them for 2 days, we dissolved the cell membrane to collect the cell lysate containing the delivered ubiquitin proteins. The NMR spectrum from the lysate (Figure 4d) matches that of a solution containing  $^{15}\text{N}$ -labeled ubiquitin (Figure 4e,f). We have analyzed the stress<sup>26</sup> and intracellular signaling process<sup>27</sup> inside HeLa cells by in-cell NMR. By using this system, we estimated the ubiquitin protein concentration from the spectrum intensity to be between 5 and 10  $\mu\text{M}$ . These findings indicate that our stamp system was highly efficient in delivering target proteins and provides a sufficient number of cells for NMR detection.

## CONCLUSIONS

We have developed a stamping system utilizing hybrid NTs composed of PEDOT/Au nanotubes for delivering proteins

into target cells. This system achieves a delivery efficiency of 89.9% across more than  $10^7$  cells, while maintaining a 97.1% viability rate. Notably, our system's capability to deliver LOx enzymes to cells demonstrates remarkable effectiveness in eradicating cancer cells with minimal impact on normal cells. This accomplishment is highly promising for the future advancement of cancer cell detection and anticancer therapies. Additionally, the successful delivery of isotope-labeled ubiquitin proteins into a significant number of cells at high concentrations has facilitated the acquisition of NMR spectra, enabling the analysis of protein interactions and functions within cells. Our system preserves protein activity during delivery as well as the delivery of multiple proteins into the cells, suggesting potential applications in cellular therapy.

## ■ ASSOCIATED CONTENT

### SI Supporting Information

The Supporting Information is available free of charge at <https://pubs.acs.org/doi/10.1021/acs.analchem.3c05331>.

Calcein flow rate through Au NT and HyNT membranes (Figure S1); images of cultured cells using PDMS molds and HyNTs stamps (Figure S2); lactate oxidase delivery into HeLa cells (Figure S3); optical and PI fluorescence images of HeLa cells (Figure S4); and flow cytometry results after ubiquitin protein delivery (Figure S5) (PDF)

## ■ AUTHOR INFORMATION

### Corresponding Authors

**Tsutomu Mikawa** – RIKEN Center for Biosystems Dynamics Research, Yokohama, Kanagawa 230-0045, Japan; [orcid.org/0000-0003-2325-5084](https://orcid.org/0000-0003-2325-5084); Email: [mikawa@riken.jp](mailto:mikawa@riken.jp)

**Takeo Miyake** – Graduate School of Information, Production and Systems, Waseda University, Kitakyushu, Fukuoka 808-0135, Japan; [orcid.org/0000-0002-7445-633X](https://orcid.org/0000-0002-7445-633X); Email: [miyake@waseda.jp](mailto:miyake@waseda.jp)

### Authors

**Bowen Zhang** – Graduate School of Information, Production and Systems, Waseda University, Kitakyushu, Fukuoka 808-0135, Japan; RIKEN Center for Biosystems Dynamics Research, Yokohama, Kanagawa 230-0045, Japan

**Bingfu Liu** – Graduate School of Information, Production and Systems, Waseda University, Kitakyushu, Fukuoka 808-0135, Japan

**Zhouji Wu** – Graduate School of Information, Production and Systems, Waseda University, Kitakyushu, Fukuoka 808-0135, Japan

**Kazuhiro Oyama** – Graduate School of Information, Production and Systems, Waseda University, Kitakyushu, Fukuoka 808-0135, Japan; RIKEN Center for Biosystems Dynamics Research, Yokohama, Kanagawa 230-0045, Japan

**Masaomi Ikari** – RIKEN Center for Biosystems Dynamics Research, Yokohama, Kanagawa 230-0045, Japan

**Hiromasa Yagi** – RIKEN Center for Biosystems Dynamics Research, Yokohama, Kanagawa 230-0045, Japan; [orcid.org/0000-0001-8059-4440](https://orcid.org/0000-0001-8059-4440)

**Naoya Tochio** – RIKEN Center for Biosystems Dynamics Research, Yokohama, Kanagawa 230-0045, Japan

**Takanori Kigawa** – RIKEN Center for Biosystems Dynamics Research, Yokohama, Kanagawa 230-0045, Japan; [orcid.org/0000-0003-0146-9719](https://orcid.org/0000-0003-0146-9719)

Complete contact information is available at: <https://pubs.acs.org/doi/10.1021/acs.analchem.3c05331>

## Notes

The authors declare no competing financial interest.

## ■ ACKNOWLEDGMENTS

This work received support from the Japan Science and Technology Agency (JST) under the PRESTO program, Grant Number JPMJPR20B8, and was also funded by the Asahi Glass Foundation. A portion of this research was carried out at the Kitakyushu Foundation for the Advancement of Industry, Science, and Technology, Semiconductor Center. It was further supported by the "Nanotechnology Platform Program" of the Ministry of Education, Culture, Sports, Science, and Technology (MEXT), Japan. Additionally, this work was partly funded by the Japan Society for the Promotion of Science (JSPS) KAKENHI, Grant No. 21H02419, awarded to T. Mikawa. The authors thank Dr. Hideto Watanabe and Tomohito Kato of Kojima Corporation for the donation of electroless solution and Ms Mutsuko Aoki of Hynts Tech Corporation for the donation of HyNTS stamps.

## ■ REFERENCES

- (1) Lee, Y.-W.; Luther, D. C.; Kretzmann, J. A.; Burden, A.; Jeon, T.; Zhai, S.; Rotello, V. M. *Theranostics* **2019**, *9* (11), 3280.
- (2) Le Saux, S.; Aubert-Pouessel, A.; Ouchait, L.; Mohamed, K. E.; Martineau, P.; Guglielmi, L.; Devoisselle, Jm.; Legrand, P.; Chopineau, J.; Morille, M. *Adv. Ther.* **2021**, *4* (6), No. 2100009.
- (3) Qin, X.; Yu, C.; Wei, J.; Li, L.; Zhang, C.; Wu, Q.; Liu, J.; Yao, S. Q.; Huang, W. *Adv. Mater.* **2019**, *31* (46), No. 1902791.
- (4) Stillger, K.; Neundorff, I. *Cell. Signalling* **2023**, *109*, No. 110796.
- (5) Kim, J. B.; Greber, B.; Araúzo-Bravo, M. J.; Meyer, J.; Park, K. I.; Zaehres, H.; Schöler, H. R. *Nature* **2009**, *461* (7264), 649–653.
- (6) Xu, J.; Fang, S.; Deng, S.; Li, H.; Lin, X.; Huang, Y.; Chung, S.; Shu, Y.; Shao, Z. *Nat. Biomed. Eng.* **2023**, *7* (3), 253–269.
- (7) Cai, L.; Wang, Y.; Yang, Y.; Wu, H. *Anal. Bioanal. Chem.* **2022**, *414*, 1987–1997.
- (8) Kang, Y.; Yeo, M.; Choi, H.; Jun, H.; Eom, S.; Park, S. G.; Yoon, H.; Kim, E.; Kang, S. *Int. J. Biol. Macromol.* **2023**, *231*, No. 123577.
- (9) Mann, G.; Sadhu, P.; Brik, A. *ChemBioChem.* **2022**, *23* (11), No. e202200122.
- (10) Gehl, J. *Acta Physiol. Scand.* **2003**, *177* (4), 437–447.
- (11) Kim, W.; Ng, J. K.; Kunitake, M. E.; Conklin, B. R.; Yang, P. J. *Am. Chem. Soc.* **2007**, *129* (23), 7228–7229.
- (12) Wang, Y.; Yang, Y.; Yan, L.; Kwok, S. Y.; Li, W.; Wang, Z.; Zhu, X.; Zhu, G.; Zhang, W.; Chen, X.; Shi, P. *Nat. Commun.* **2014**, *5* (1), No. 4466.
- (13) Yum, K.; Na, S.; Xiang, Y.; Wang, N.; Yu, M.-F. *Nano Lett.* **2009**, *9* (5), 2193–2198.
- (14) Lee, J.; Choi, S.; Bae, S. J.; Yoon, S. M.; Choi, J. S.; Yoon, M. *Nanoscale* **2013**, *5* (21), 10275–10282.
- (15) Peer, E.; Artzy-Schnirman, A.; Gepstein, L.; Sivan, U. *ACS Nano* **2012**, *6* (6), 4940–4946.
- (16) Wen, R.; Zhang, A.-h.; Liu, D.; Feng, J.; Yang, J.; Xia, D.; Wang, J.; Li, C.; Zhang, T.; Hu, N.; et al. *ACS Appl. Mater. Interfaces* **2019**, *11* (47), 43936–43948.
- (17) Park, S.; Kim, Y.-S.; Kim, W. B.; Jon, S. *Nano Lett.* **2009**, *9* (4), 1325–1329.
- (18) Xie, X.; Xu, A. M.; Leal-Ortiz, S.; Cao, Y.; Garner, C. C.; Melosh, N. A. *ACS Nano* **2013**, *7* (5), 4351–4358. VanDersarl, J. J.; Xu, A. M.; Melosh, N. A. *Nano Lett.* **2012**, *12* (8), 3881–3886.

(19) Zhang, B.; Shi, Y.; Miyamoto, D.; Nakazawa, K.; Miyake, T. *Sci. Rep.* **2019**, *9* (1), No. 6806.

(20) Zhang, B.; Zheng, D.; Yiming, S.; Oyama, K.; Ito, M.; Ikari, M.; Kigawa, T.; Mikawa, T.; Miyake, T. *Small Sci.* **2021**, *1* (12), No. 2100069.

(21) Shitanda, I.; Takamatsu, K.; Niiyama, A.; Mikawa, T.; Hoshi, Y.; Itagaki, M.; Tsujimura, S. *J. Power Sources* **2019**, *436*, No. 226844.

(22) Inomata, K.; Kamoshida, H.; Ikari, M.; Ito, Y.; Kigawa, T. *Chem. Commun.* **2017**, *53* (81), 11245–11248.

(23) Yin, S.; Liu, X.; Kaji, T.; Nishina, Y.; Miyake, T. *Biosens. Bioelectron.* **2021**, *179*, No. 113107.

(24) Shitanda, I.; Morigayama, Y.; Iwashita, R.; Goto, H.; Aikawa, T.; Mikawa, T.; Hoshi, Y.; Itagaki, M.; Matsui, H.; Tokito, S. *J. Power Sources* **2021**, *489*, No. 229533.

(25) Shitanda, I.; Mitsumoto, M.; Loew, N.; Yoshihara, Y.; Watanabe, H.; Mikawa, T.; Tsujimura, S.; Itagaki, M.; Motosuke, M. *Electrochim. Acta* **2021**, *368*, No. 137620.

(26) Hembram, D. S. S.; Haremake, T.; Hamatsu, J.; Inoue, J.; Kamoshida, H.; Ikeya, T.; Mishima, M.; Mikawa, T.; Hayashi, N.; Shirakawa, M.; Ito, Y. *Biochem. Biophys. Res. Commun.* **2013**, *438* (4), 653–659.

(27) Ikari, M.; Yagi, H.; Kasai, T.; Inomata, K.; Ito, M.; Higuchi, K.; Matsuda, N.; Ito, Y.; Kigawa, T. *JACS Au* **2023**, *3* (6), 1658–1669.